Chapter 16

The Asymmetrical Dual Three-Phase Induction Machine and the MBPC in the Speed Control

Raúl Igmar Gregor Recalde

Additional information is available at the end of the chapter

http://dx.doi.org/10.5772/50559

1. Introduction

Recent research has focused on exploring the advantages of multiphase[1] machines over conventional three-phase systems, including lower torque pulsations, less DC-link current harmonics, higher overall system reliability, and better power distribution per phase [1]. Among these multiphase drives, the asymmetrical dual three-phase machines with two sets of three-phase stator windings spatially shifted by 30 electrical degrees and isolated neutral points is one of the most widely discussed topologies and found industrial application in more-electric aircraft, electrical and hybrid vehicles, ship propulsion, and wind power systems [2]. This asymmetrical dual three-phase machines is a continuous system which can be described by a set of differential equations. A methodology that simplifies the modeling is based on the vector space decomposition (VSD) theory introduced in [3] to transform the original six-dimensional space of the machine into three two-dimensional orthogonal subspaces in stationary reference frame $(\alpha - \beta)$, $(x - y)$ and $(z_1 - z_2)$. From the VSD approach, can be emphasized that the electromechanical energy conversion variables are mapped in the $(\alpha - \beta)$ subspace, meanwhile the current components in the $(x - y)$ subspace represent supply harmonics of the order $6n \pm 1$ ($n = 1, 3, 5, ...$) and only produce losses, so consequently should be controlled to be as small as possible. The voltage vectors in the $(z_1 - z_2)$ are zero due to the separated neutral configuration of the machine, therefore this subspace has no influence on the control [4].

Model-based predictive control (MBPC) and multiphase drives have been explored together in [5, 6], showing that predictive control can provide enhanced performance for multiphase drives. In [7, 8], different variations of the predictive current control techniques are proposed to minimize the error between predicted and reference state variables, at the expense of increased switching frequency of the insulated-gate bipolar transistor (IGBTs). On the other hand are proposed control strategies based on sub-optimal solutions restricted the available voltage vectors for multiphase drive applications aiming at reducing the computing cost and

[1] The multiphase term, regards more than three phase windings placed in the same stator of the electric machine.

improving the drive performance [9]. This chapter wide the concept of the MBPC techniques to the speed control of a dual three-phase induction machine, by using an Kalman Filter (KF) to improve the estimation of states through an optimal estimation of the rotor current. The KF is an efficient recursive filter that estimates the internal state of a dynamic system from a series of noisy measurements. Its purpose is to use measurements that are observed over time that contain noise (random variations) and other inaccuracies (including modeling errors), and produce values that tend to be closer to the true values of the measurements and their associated calculated values. This feature is an attractive solution in the predictive control of induction machines based on the model, mainly if not precisely known internal parameters of the drive, and the measurement of the state variables are perturbed by gaussian noise.

The chapter includes simulation results of the current control based on a predictive model of the asymmetrical dual three-phase induction machine and proposes a new approach to speed control based on MBPC technique. The results provided confirm the feasibility of the speed control scheme for multi-phase machines. The rest of the chapter is organized as follows. Section 2 introduces an asymmetrical dual three-phase AC drive used for simulations. Section 3 details the general principles of the predictive current control method for AC drives. Section 4 shows the simulation results obtained from the inner loop of predictive current control and proposed a new approach to speed control for the dual three-phase induction machine, on the other hand presents a discussion of the obtained results from the proposed approach. The chapter ends with Section 5 where the conclusions are presented.

2. The asymmetrical dual three-phase AC drive

The asymmetrical dual three-phase induction machine is supplied by a 6-phase voltage source inverter (VSI) and a Dc Link, as shown in Figure 1. This six-phase machine is a continuous system which can be described by a set of differential equations. A methodology that simplifies the modeling is based on the vector space decomposition (VSD) theory introduced in [3] to transform the original six-dimensional space of the machine into three

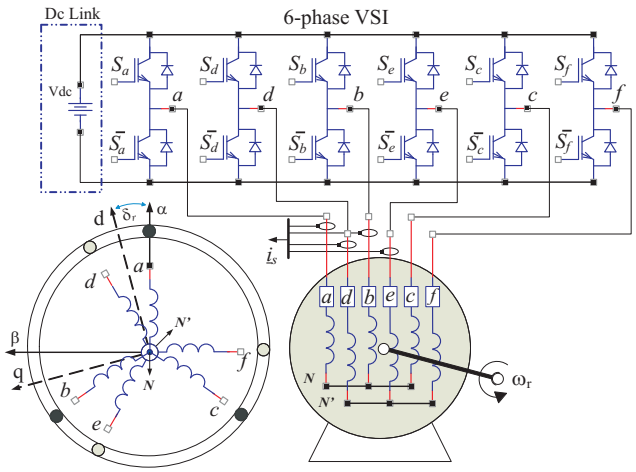

Figure 1. A general scheme of an asymmetrical dual three-phase drive

two-dimensional orthogonal subspaces in stationary reference frame $(\alpha - \beta)$, $(x - y)$ and $(z_1 - z_2)$, by means of a 6×6 transformation matrix using an amplitude invariant criterion:

$$\mathbf{T} = \frac{1}{3}\begin{bmatrix} 1 & \frac{\sqrt{3}}{2} & -\frac{1}{2} & -\frac{\sqrt{3}}{2} & -\frac{1}{2} & 0 \\ 0 & \frac{1}{2} & \frac{\sqrt{3}}{2} & \frac{1}{2} & -\frac{\sqrt{3}}{2} & -1 \\ 1 & -\frac{\sqrt{3}}{2} & -\frac{1}{2} & \frac{\sqrt{3}}{2} & -\frac{1}{2} & 0 \\ 0 & \frac{1}{2} & -\frac{\sqrt{3}}{2} & \frac{1}{2} & \frac{\sqrt{3}}{2} & -1 \\ 1 & 0 & 1 & 0 & 1 & 0 \\ 0 & 1 & 0 & 1 & 0 & 1 \end{bmatrix} \tag{1}$$

The VSI has a discrete nature and has a total number of $2^6 = 64$ different switching states defined by six switching functions corresponding to the six inverter legs $[S_a, S_d, S_b, S_e, S_c, S_f]$, where $\mathbf{S}_i \in \{0, 1\}$. The different switching states and the voltage of the DC link (Vdc) define the phase voltages which can in turn be mapped to the $(\alpha - \beta) - (x - y)$ space according to the VSD approach. Consequently, the 64 different on/off combinations of the six VSI legs lead to 64 space vectors in the $(\alpha - \beta)$ and $(x - y)$ subspaces. Figure 2 shows the active vectors in the $(\alpha - \beta)$ and $(x - y)$ subspaces, where each vector switching state is identified using the switching function by two octal numbers corresponding to the binary numbers $[S_a S_b S_c]$ and $[S_d S_e S_f]$, respectively. For the sake of conciseness, the 64 VSI switching vectors will be usually referred as voltage vectors, or just vectors, in what follows. It must be noted that the 64 possibilities imply only 49 different vectors in the $(\alpha - \beta) - (x - y)$ space. Nevertheless, redundant vectors should be considered as different vectors because they have a different impact on the switching frequency even though they generate identical torque and losses in the six-phase machine.

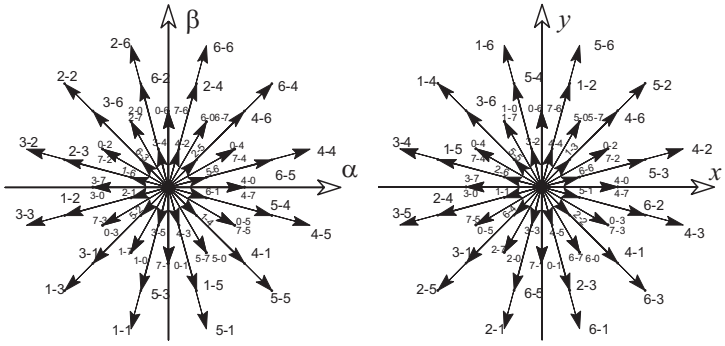

Figure 2. Voltage vectors and switching states in the $(\alpha - \beta)$ and $(x - y)$ subspaces for a 6-phase asymmetrical VSI

To represent the stationary reference frame $(\alpha - \beta)$ in dynamic reference $(d - q)$, a rotation transformation must be used. This transformation is given by:

$$\mathbf{T}_{dq} = \begin{bmatrix} cos\,(\delta_r) & -sin\,(\delta_r) \\ sin\,(\delta_r) & cos\,(\delta_r) \end{bmatrix} \tag{2}$$

where δ_r is the rotor angular position referred to the stator as shown in Figure 1.

2.1. Machine model in the $(\alpha - \beta)$ subspace

The asymmetrical dual three-phase machine model can be obtained using a specific and convenient choice of state-space variables, for example, stator and rotor currents. Thus the six-phase machine can be modelled in a stationary reference frame according to the VSD approach as:

$$[\mathbf{u}]_{\alpha\beta} = [\mathbf{G}] \frac{d}{dt} [\mathbf{x}]_{\alpha\beta} + [\mathbf{F}] [\mathbf{x}]_{\alpha\beta} \tag{3}$$

$$[\mathbf{u}]_{\alpha\beta} = \begin{bmatrix} u_{\alpha s} & u_{\beta s} & 0 & 0 \end{bmatrix}^T ; [\mathbf{x}]_{\alpha\beta} = \begin{bmatrix} i_{\alpha s} & i_{\beta s} & i_{\alpha r} & i_{\beta r} \end{bmatrix}^T \tag{4}$$

where $[\mathbf{u}]_{\alpha\beta}$ is the input vector, $[\mathbf{x}]_{\alpha\beta}$ is the state vector and $[\mathbf{F}]$ and $[\mathbf{G}]$ are matrices that define the dynamics of the electrical drive that for this set of state variables are:

$$[\mathbf{F}] = \begin{bmatrix} R_s & 0 & 0 & 0 \\ 0 & R_s & 0 & 0 \\ 0 & \omega_r \cdot L_m & R_r & \omega_r \cdot L_r \\ -\omega_r \cdot L_m & 0 & -\omega_r \cdot L_r & R_r \end{bmatrix} ; [\mathbf{G}] = \begin{bmatrix} L_s & 0 & L_m & 0 \\ 0 & L_s & 0 & L_m \\ L_m & 0 & L_r & 0 \\ 0 & L_m & 0 & L_r \end{bmatrix} \tag{5}$$

where ω_r is the rotor angular speed, and the electrical parameters of the machine are the stator and rotor resistances R_s, R_r, the stator and rotor inductances $L_s = L_{ls} + L_m$, $L_r = L_{lr} + L_m$, the stator and rotor leakage inductances L_{ls}, L_{lr} and the magnetization inductance L_m. Using selected state-space variables and amplitude invariant criterion in the transformation, the mechanical part of the drive is given by the following equations:

$$T_e = 3.P \left(\psi_{\beta r} i_{\alpha r} - \psi_{\alpha r} i_{\beta r} \right) \tag{6}$$

$$J_i \frac{d}{dt} \omega_r + B_i \omega_r = P \left(T_e - T_L \right) \tag{7}$$

where T_e is the generated torque, T_L the load torque, P the number of pair of poles, J_i the inertia coefficient, B_i the friction coefficient and $\psi_{\alpha\beta r}$ the rotor flux.

The $(\alpha - \beta)$[2] axes are selected in such a manner that they coincide with the plane of rotation of the airgap flux. Therefore, these variables will are associated with the production of the airgap flux in the machine and with the electromechanical energy conversion related [3].

2.2. Machine model in the $(x - y)$ subspace

Because the $(x - y)$ subspace is orthogonal to the $(\alpha - \beta)$ subspace, the projected variables in this subspace will do not contribute to the airgap flux, and therefore are not related to energy conversion. This model are limited only by the stator resistance and stator leakage inductance, as shown in the following equation:

$$\begin{bmatrix} u_{xs} \\ u_{ys} \end{bmatrix} = \begin{bmatrix} L_{ls} & 0 \\ 0 & L_{ls} \end{bmatrix} \frac{d}{dt} \begin{bmatrix} i_{xs} \\ i_{ys} \end{bmatrix} + \begin{bmatrix} R_s & 0 \\ 0 & R_s \end{bmatrix} \begin{bmatrix} i_{xs} \\ i_{ys} \end{bmatrix} \tag{8}$$

[2] It can be noted that $(\alpha - \beta)$ equations are similar to those of a three-phase machine while that, as will be seen in the following section, the $(x - y)$ equations do not link the rotor side and consequently do not influence the machine dynamics but are source of Joule losses in the machine.

3. Predictive model

The machine model must be discretized in order to be of use as a predictive model. Taking into account that the electromechanical energy conversion involves only quantities in the $(\alpha - \beta)$ subspace, the predictive model could be simplified, discarding the $(x - y)$ subspace. Assuming the asymmetrical dual three-phase induction machine model (see Equation 3) and using the following state components ($x_1 = i_{\alpha s},\ x_2 = i_{\beta s},\ x_3 = i_{\alpha r},\ x_4 = i_{\beta r}$), the resulting equations can be written as:

$$\begin{aligned}
\dot{x_1} &= c_3\left(R_r x_3 + \omega_r x_4 L_r + \omega_r x_2 L_m\right) + c_2\left(u_{\alpha s} - R_s x_1\right) \\
\dot{x_2} &= c_3\left(R_r x_4 - \omega_r x_3 L_r - \omega_r x_1 L_m\right) + c_2\left(u_{\beta s} - R_s x_2\right) \\
\dot{x_3} &= c_4\left(-R_r x_3 - \omega_r x_4 L_r - \omega_r x_2 L_m\right) + c_3\left(-u_{\alpha s} + R_s x_1\right) \\
\dot{x_4} &= c_4\left(-R_r x_4 + \omega_r x_3 L_r + \omega_r x_1 L_m\right) + c_3\left(-u_{\beta s} + R_s x_2\right)
\end{aligned} \tag{9}$$

where c_1-c_4 are constant coeficients defined as:

$$c_1 = L_s \cdot L_r - L_m^2,\ c_2 = \frac{L_r}{c_1},\ c_3 = \frac{L_m}{c_1},\ c_4 = \frac{L_s}{c_1} \tag{10}$$

Stator voltages are related to the control input signals through the inverter model. The simplest model has been selected for this case study for the sake of speeding up the optimization process. Then if the gating signals are arranged in vector $\mathbf{S} = \left[S_a,\ S_d,\ S_b,\ S_e,\ S_c,\ S_f\right] \in \mathbf{R}^6$, with $\mathbf{R} = \{0, 1\}$ the stator voltages are obtained from:

$$\mathbf{M} = \frac{1}{3}\begin{bmatrix} 2 & 0 & -1 & 0 & -1 & 0 \\ 0 & 2 & 0 & -1 & 0 & -1 \\ -1 & 0 & 2 & 0 & -1 & 0 \\ 0 & -1 & 0 & 2 & 0 & -1 \\ -1 & 0 & -1 & 0 & 2 & 0 \\ 0 & -1 & 0 & -1 & 0 & 2 \end{bmatrix} \cdot \mathbf{S}^T \tag{11}$$

An ideal inverter converts gating signals to stator voltages that can be projected to $(\alpha - \beta)$ and $(x - y)$ axes and gathered in a row vector $\mathbf{U}_{\alpha\beta xys}$ computed as:

$$\mathbf{U}_{\alpha\beta xys} = \left[u_{\alpha s},\ u_{\beta s},\ u_{xs},\ u_{ys},\ 0,\ 0\right]^T = Vdc \cdot \mathbf{T} \cdot \mathbf{M} \tag{12}$$

being Vdc the Dc Link voltage and superscript (^{T}) indicates the transposed matrix. Combining Equations 9-12 a nonlinear set of equations arises that can be written in state space form:

$$\begin{aligned}
\dot{\mathbf{X}}(t) &= f\left(\mathbf{X}(t),\ \mathbf{U}(t)\right) \\
\mathbf{Y}(t) &= \mathbf{C}\mathbf{X}(t)
\end{aligned} \tag{13}$$

with state vector $\mathbf{X}(t) = [x_1,\ x_2,\ x_3,\ x_4]^T$, input vector $\mathbf{U}(t) = \left[u_{\alpha s},\ u_{\beta s}\right]$, and output vector $\mathbf{Y}(t) = [x_1,\ x_2]^T$. The components of vectorial function f and matrix $\mathbf{C}$ are obtained in a straightforward manner from Equation 9 and the definitions of state and output vector.

Model (Equation 13) must be discretized in order to be of use for the predictive controller. A forward Euler method is used to keep a low computational burden. As a consequence the resulting equations will have the needed digital control form, with predicted variables depending just on past values and not on present values of variables. This leads to the following equations:

$$\begin{aligned} \hat{\mathbf{X}}(k+1|k) &= \mathbf{X}(k) + T_m f\left(\mathbf{X}(k),\, \mathbf{U}(k)\right) \\ \mathbf{Y}(k) &= \mathbf{C}\mathbf{X}(k) \end{aligned} \tag{14}$$

denoting by (k) the current sample, T_m the sampling time and being $\hat{\mathbf{X}}(k+1|k)$ a prediction of the future next-sample state made at sample time (k).

3.1. Kalman Filter design

Kalman Filter is an optimal recursive estimation algorithm based on the state-space concepts and suitable for digital computer implementation. That is, it is an optimal estimator for computing the conditional mean and covariance of the probability distribution of the state of a linear stochastic system with uncorrelated gaussian process and measurement noise. The algorithm minimizes the estimate error of the states by utilizing knowledge of system and measurements dynamic, assuming statistics of system noises and measurement errors, considering initial condition information [10]. Considering uncorrelated gaussian process and measurement noise, Equations 14 can be written as:

$$\begin{aligned} \hat{\mathbf{X}}(k+1|k) &= \mathbf{A}\mathbf{X}(k) + \mathbf{B}\mathbf{U}(k) + \mathbf{H}\varpi(k) \\ \mathbf{Y}(k) &= \mathbf{C}\mathbf{X}(k) + \nu(k) \end{aligned} \tag{15}$$

the matrices $\mathbf{A}$, $\mathbf{B}$ and $\mathbf{C}$ are obtained in a straightforward manner from Equation 14 and the definitions of state and output vector, $\mathbf{H}$ is the noise-weight matrix, $\varpi(k)$ is the process noise matrix, and $\nu(k)$ is the measurement noise matrix. The covariance matrices R_ϖ and R_ν of these noises are defined in function to the expected value $E\{\cdot\}$ as:

$$R_\varpi = cov(\varpi) = E\left\{\varpi \cdot \varpi^T\right\}; R_\nu = cov(\nu) = E\left\{\nu \cdot \nu^T\right\} \tag{16}$$

3.1.1. Reduced-order state estimation

In the state space description of Equation 14 only stator currents, voltages and mechanical speed are measured. Stator voltages are easily predicted from gating commands issued to the VSI, rotor current, however, is not directly measured. This difficulty can be overcome by means of estimating the rotor current using the concept of reduced-order estimators. The reduced-order estimator provide an estimate for only the unmeasured part of state vector, then, the evolution of states can be written as:

$$\begin{bmatrix} \mathbf{X}_a(k+1|k) \\ \cdots \\ \mathbf{X}_b(k+1|k) \end{bmatrix} = \begin{bmatrix} \overline{\mathbf{A}}_{11} & \vdots & \overline{\mathbf{A}}_{12} \\ \cdots & \cdots & \cdots \\ \overline{\mathbf{A}}_{21} & \vdots & \overline{\mathbf{A}}_{22} \end{bmatrix} \begin{bmatrix} \mathbf{X}_a(k) \\ \cdots \\ \mathbf{X}_b(k) \end{bmatrix} + \begin{bmatrix} \overline{\mathbf{B}}_1 \\ \cdots \\ \overline{\mathbf{B}}_2 \end{bmatrix} \mathbf{U}_{\alpha\beta s}(k)$$

$$\mathbf{Y}(k) = \begin{bmatrix} \overline{\mathbf{I}} \vdots \overline{\mathbf{0}} \end{bmatrix} \begin{bmatrix} \mathbf{X}_a(k) \\ \cdots \\ \mathbf{X}_b(k) \end{bmatrix} \tag{17}$$

where $\mathbf{I}$ is the identity matrix of order 2x2, $\mathbf{X}_a = \left[i_{\alpha s}(k)\ i_{\beta s}(k) \right]^T$ is the portion directly measured, which is $\mathbf{Y}(k)$, $\mathbf{X}_b = \left[i_{\alpha r}(k)\ i_{\beta r}(k) \right]^T$ is the remaining portion to be estimated, and $\overline{\mathbf{A}}$ and $\overline{\mathbf{B}}$ are matrices obtained in a straightforward manner from Equation 15 and are represented according to the following matrices:

$$\overline{\mathbf{A}} = \begin{bmatrix} (1 - T_m.c_2.R_s) & T_m.c_3.L_m.\omega_r & \vdots & T_m.c_3.R_r & T_m.c_3.L_r.\omega_r \\ -T_m.c_3.L_m.\omega_r & (1 - T_m.c_2.R_s) & \vdots & -T_m.c_3.L_r.\omega_r & T_m.c_3.R_r \\ \cdots & \cdots & \cdots & \cdots & \cdots \\ T_m.c_3.R_s & -T_m.c_4.L_m.\omega_r & \vdots & (1 - T_m.c_4.R_r) & -T_m.c_4.L_r.\omega_r \\ T_m.c_4.L_m.\omega_r & T_m.c_3.R_s & \vdots & T_m.c_4.L_r.\omega_r & (1 - T_m.c_4.R_r) \end{bmatrix}$$

$$\overline{\mathbf{B}} = \begin{bmatrix} T_m.c_2 & 0 \\ 0 & T_m.c_2 \\ \cdots & \cdots \\ -T_m.c_3 & 0 \\ 0 & -T_m.c_3 \end{bmatrix} \tag{18}$$

The portion describing the dynamics of the unmeasured states can be written as:

$$\mathbf{X}_b(k+1|k) = \overline{\mathbf{A}}_{22}\mathbf{X}_b(k) + \overline{\mathbf{A}}_{21}\mathbf{X}_a(k) + \overline{\mathbf{B}}_2\mathbf{U}_{\alpha\beta s}(k) \tag{19}$$

where the last two terms on the right are known and can be considered as an input into the $\mathbf{X}_b$ dinamics. The $\mathbf{X}_a$ portion may be expressed as:

$$\mathbf{X}_a(k+1|k) - \overline{\mathbf{A}}_{11}\mathbf{X}_a(k) - \overline{\mathbf{B}}_1\mathbf{U}_{\alpha\beta s}(k) = \overline{\mathbf{A}}_{12}\mathbf{X}_b(k) \tag{20}$$

Note in Equation 20 that this equation represent a relationship between a measured quantity on the left and the unknown state vector on the right. Therefore, the dynamics of the reduced-order estimator ecuations are:

$$\begin{aligned} \hat{\mathbf{X}}_b(k+1|k) = {} & (\overline{\mathbf{A}}_{22} - \mathbf{K}_e\overline{\mathbf{A}}_{12})\hat{\mathbf{X}}_b(k) + \mathbf{K}_e\mathbf{Y}(k+1) + \\ & (\overline{\mathbf{A}}_{21} - \mathbf{K}_e\overline{\mathbf{A}}_{11})\mathbf{Y}(k) + (\overline{\mathbf{B}}_2 - \mathbf{K}_e\overline{\mathbf{B}}_1)\mathbf{U}_{\alpha\beta s}(k) \end{aligned} \tag{21}$$

where, $\mathbf{K}_e$ represents the KF gain matrix based on the covariance of the noise.

3.1.2. Kalman Filter gain matrix evaluation

The KF gain matrix ($\mathbf{K}_e$) is recalculated at each sampling time recursive manner as:

$$\mathbf{K}_e(k) = \mathbf{\Gamma}(k) \cdot \mathbf{C}^T R_v \tag{22}$$

where $\mathbf{\Gamma}$ is the covariance of the new estimate and is a function of the old estimate covariance (φ) as follows:

$$\mathbf{\Gamma}(k) = \varphi(k) - \varphi(k) \cdot \mathbf{C}^T(\mathbf{C} \cdot \varphi(k) \cdot \mathbf{C}^T + R_v)^{-1} \cdot \mathbf{C} \cdot \varphi(k) \tag{23}$$

From the state equation which includes the process noise it is possible to obtain a correction of the covariance of the state estimate as:

$$\varphi(k+1) = \mathbf{A} \cdot \mathbf{\Gamma}(k) \cdot \mathbf{A}^T + \mathbf{H} \cdot R_\omega \cdot \mathbf{H}^T \tag{24}$$

This completes the required relations for the optimal state estimation. Thus $\mathbf{K}_e$ provides the minimum estimation errors, given a knowledge of the process noise magnitude (R_ω), the measurement noise magnitude (R_ν), and the covariance initial condition ($\varphi(0)$) [11].

3.2. Current control loop

The current control loop, based on the MBPC technique avoids the use of modulation techniques since a single switching vector is applied during the whole switching period. The MBPC technique selects the control actions through solving an optimization problem at each sampling period. A model of the real system, is used to predict its output. This prediction is carried out for each possible output, or switching vector, of the six-phase inverter to determine which one minimizes a defined cost function. The proposed scheme is shown in Figure 3.

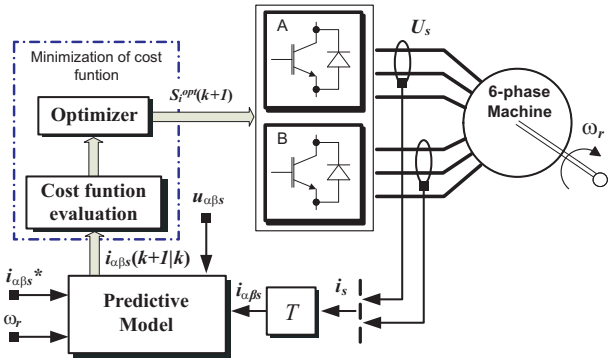

Figure 3. Current control loop based on the MBPC technique

3.2.1. Cost function

The cost function should include all aspects to be optimized. In the current predictive control applied to the asymmetrical dual three-phase induction machine, the most important feature to be optimized are the tracking errors of the stator currents in the $(\alpha - \beta)$ subspace for a next sampling time, since this variables are related to the electromechanical conversion. To minimize the prediction errors at each sampling time k it enough utilize a simple term as:

$$J = \| \hat{e}_{i\alpha s}(k+1|k) + \hat{e}_{i\beta s}(k+1|k) \|^2 \leftrightarrow \begin{cases} \hat{e}_{i\alpha s}(k+1|k) = i^*_{\alpha s}(k+1) - \hat{i}_{\alpha s}(k+1|k) \\ \hat{e}_{i\beta s}(k+1|k) = i^*_{\beta s}(k+1) - \hat{i}_{\beta s}(k+1|k) \end{cases} \tag{25}$$

where $\| \ . \ \|$ denotes the vector modulus, i^*_s is a vector containing the reference for the stator currents and $\hat{i}_s(k+1|k)$ is the prediction of the stator currents calculated from measured and estimated states and the voltage vector $U_{\alpha\beta s}(k)$ as shown in Equation 20. Figure 4 (a) shows the all projection of the stator current predictions calculated from the prediction model. The current control selects the control vector that minimizes the cost function at each sampling time. Figure 4 (b) shows the selection of the optimal vector based on a minimization of prediction errors.

More complicated cost functions can be devised for instance to minimize harmonic content, VSI switching losses, torque and flux and/or active and reactive power. Also, in multi-phase

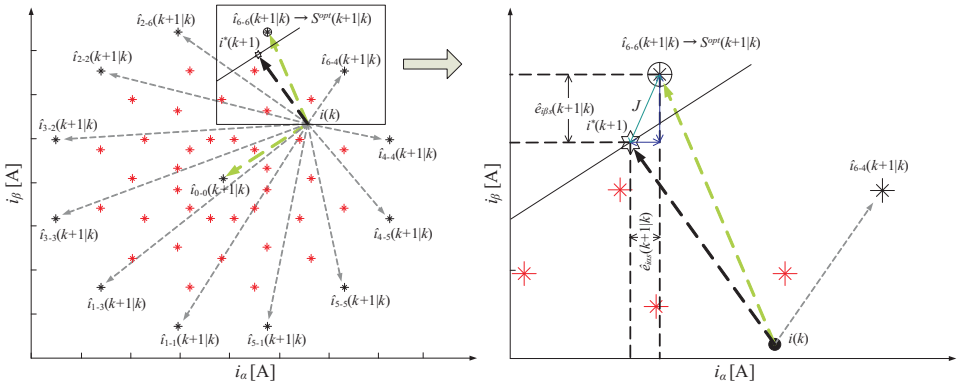

(a) Projection of the stator currents prediction in stationary reference frame $(\alpha - \beta)$

(b) Evaluation of the cost function (J) and selection of the optimal vector (S^{opt})

Figure 4. Minimization of tracking error in stator currents in stationary reference frame $(\alpha - \beta)$

drives stator current can be decomposed in subspaces in different ways. An appropriate decomposition allow to put more emphasis on harmonic reduction as will be shown in the case study for a six-phase motor drive [5, 12]. The more relevant cost functions are shown in Table 1. The superscript $(^*)$ denote the reference value and the terms involved in each cost function are detailed in the Table 2.

Controlled variables	Cost functions (J)
Currents (α-β) and harmonic $(x-y)$	$\|\|i_\alpha^* - i_\alpha\| + \|i_\beta^* - i_\beta\|\|^2 + \lambda.\|\|i_x^* - i_x\| + \|i_y^* - i_y\|\|$
Active and reactive power	$\|Q_{in}\| + \|P_{in}^* - P_{in}\|$
Torque and flux	$\|T_e^* - T_e\| + \lambda\|\|\psi_s^*\| - \|\psi_s\|\|$
Currents (α-β) and voltage balance	$\|\|i_\alpha^* - i_\alpha\| + \|i_\beta^* - i_\beta\|\| + \lambda.\|V_{c1} - V_{c2}\|$
Currents (α-β) and VSI switching losses	$\|\|i_\alpha^* - i_\alpha\| + \|i_\beta^* - i_\beta\|\| + \lambda.N_s$

Table 1. Possible cost functions in function to the controlled variables

Variable	Description
i_α	Measured α current
i_β	Measured β current
i_x	Measured x current
i_y	Measured y current
Q_{in}	Reactive power
P_{in}	Active power
T_e	Torque
ψ_s	Flux of the stator
λ	Weighting factor
V_{c1}, V_{c2}	Voltages on each capacitor (VSI balanced)
N_s	Number of switches

Table 2. Description of the terms involved in each cost function of the Table 1

3.2.2. Optimizer

The predictive model should be used 64 times to consider all possible voltage vectors. However, the redundancy of the switching states results in only 49 different vectors (48 active and 1 null) as shown on Figure 2. This consideration is commonly known as the optimal solution. The number of voltage vectors to evaluate the predictive model can be further reduced if only the 12 outer vectors (the largest ones) are considered. This assumption is commonly used if sinusoidal output voltage is required and it is not necessary to synthesize $(x-y)$ components. In this way, the optimizer can be implemented using only 13 possible stator voltage vectors[3]. This way of proceeding increases the speed at which the optimizer can be run, allowing decreasing the sampling time at the cost of losing optimality. A detailed study of the implications of considering the optimal solution can be found at [6]. For a generic multi-phase machine, where f is the number of phase and ε the search space (49 or 13 vectors), the control algorithm proposed produces the optimum gating signal combination S^{opt} as follows:

Algorithm 1 Proposed algorithm

comment: Compute the covariance matrix. Equation 23
$\mathbf{\Gamma}(k) = \varphi(k) - \varphi(k) \cdot \mathbf{C}^T (\mathbf{C} \cdot \varphi(k) \cdot \mathbf{C}^T + R_v)^{-1} \cdot \mathbf{C} \cdot \varphi(k)$
comment: Compute the KF gain matrix. Equation 22
$\mathbf{K}_e(k) = \mathbf{\Gamma}(k) \cdot \mathbf{C}^T R_v$
comment: Optimization algorithm
$J_o := \infty, i := 1$
while $i \leq \varepsilon$ **do**
  $\mathbf{S}_i \leftarrow \mathbf{S}_{i,j} \; \forall \, j = 1, ..., f$
  comment: Compute stator voltages. Equation 12
  $U_{\alpha\beta xys} = \left[u_{\alpha s},\, u_{\beta s},\, u_{xs},\, u_{ys},\, 0,\, 0 \right]^T = Vdc \cdot \mathbf{T} \cdot \mathbf{M}$
  comment: Compute a prediction of the state. Equation 15
  $\hat{\mathbf{X}}(k+1|k) = \mathbf{A}\mathbf{X}(k) + \mathbf{B}\mathbf{U}(k) + \mathbf{H}\varpi(k)$
  comment: Compute the cost function. Equation 25
  $J = \| \, \hat{e}_{i\alpha s}(k+1|k) + \hat{e}_{i\beta s}(k+1|k) \, \|^2$
  if $J < J_o$ **then**
    $J_o \leftarrow J, \mathbf{S}^{opt} \leftarrow \mathbf{S}_i$
  end if
  $i := i + 1$
end while
comment: Compute the correction of the covariance matrix. Equation 24
$\varphi(k+1) = \mathbf{A} \cdot \mathbf{\Gamma}(k) \cdot \mathbf{A}^T + \mathbf{H} \cdot R_\varpi \cdot \mathbf{H}^T$

4. Simulation results

A Matlab/Simulink simulation environment has been designed for the VSI-fed asynchronous asymmetrical dual three-phase induction machine, and simulations have been done to prove the efficiency of the scheme proposed. Numerical integration using fourth order Runge-Kutta

[3] 12 active, corresponding to the largest vectors in the $(\alpha - \beta)$ subspace and the smallest ones in the $(x-y)$ subspace plus a zero vector.

algorithm has been applied to compute the evolution of the state variables step by step in the time domain. Table 3 shows the electrical and mechanical parameters for the asymmetrical dual three-phase induction machine.

Parameter		Value
Stator resistance	R_s (Ω)	1.63
Rotor resistance	R_r (Ω)	1.08
Stator inductance	L_s (H)	0.2792
Rotor inductance	L_r (H)	0.2886
Mutual inductance	L_m (H)	0.2602
Inertia	J_i (kg.m^2)	0.109
Pairs of poles	P	3
Friction coefficient	B (kg.m^2/s)	0.021
Nominal frequency	ω_a (Hz)	50

Table 3. Parameters of the asymmetrical dual three-phase induction machine

Computer simulations allow valuing the effectiveness of the proposed control system under unload and full-load conditions, with respect to the mean squared error (MSE) of the speed and stator current tracking. In all cases is considered a sampling frequency of 6.5 kHz, and that the initial conditions of the covariance matrix ($\varphi(0)$), and the process and measurement noise, are known. The Kalman Filter has been started with the following initial conditions; $\varphi(0) = diag\left[1\ 1\ 1\ 1\right]$, in order to indicate that the initial uncertainty (rms) of the state variables is 1 A. Because $\varphi(k)$ is time varying, the KF gain is sensitive to this initial condition estimate during the initial transient, but the steady final values are not affected [11]. The magnitudes of the process noise (R_ω) and measurement noise (R_ν) are known and are generate using a Random Source block of the Simulink Signal Processing Blockset, assuming the following values, $R_\omega = 15 \times 10^{-3}$ and $R_\nu = 25 \times 10^{-3}$, respectively.

4.1. Efficiency of current control loop

A series of simulation tests are performed in order to verify the efficiency of current control loop in three points of operation of the machine. Figure 5 shows the current tracking in stationary reference frame $(\alpha - \beta)$ and $(x - y)$ subspaces considering sub-optimal solution in the optimization process (12 active and 1 null vectors). The predicted stator current in the α component is shown in the upper side (zoom graphs and green curves). For all cases of analysis efficiency is measured with respect to the MSE of the currents tracking in $(\alpha - \beta)$-$(x - y)$ subspaces and the total harmonic distortion (THD), defined as the ratio of the sum of the powers of all harmonic components to the power of the fundamental frequency, obtained from the Powergui-Continuous Simulink block. A 2.5 A reference stator current at 12 Hz is established for the case of Figure 5 (a). Figure 5 (b) shows the current tracking in the $(\alpha - \beta)$ and $(x - y)$ subspaces using a 2 A reference stator current at 18 Hz and Figure 5 (c) shows the current tracking in stationary reference frame using a 1.5 A reference stator current at 36 Hz. Table 4 summarizes the results of the three previous trials where are considered different amplitudes and angular frequencies for the reference current.

From the obtained results can be emphasized as follows:

Method	Test	MSE_α, MSE_β	MSE_x, MSE_y	THD_α, THD_β
MBPC	(a)	0.2105, 0.2322	0.9298, 0.9304	7.1330,7.5969
	(b)	0.1989, 0.2141	1.0957, 1.0885	10.3610, 11.8192
	(c)	0.2287, 0.2348	1.2266, 1.3102	15.8951, 17.4362

Table 4. Simulation results obtained from Figure 5

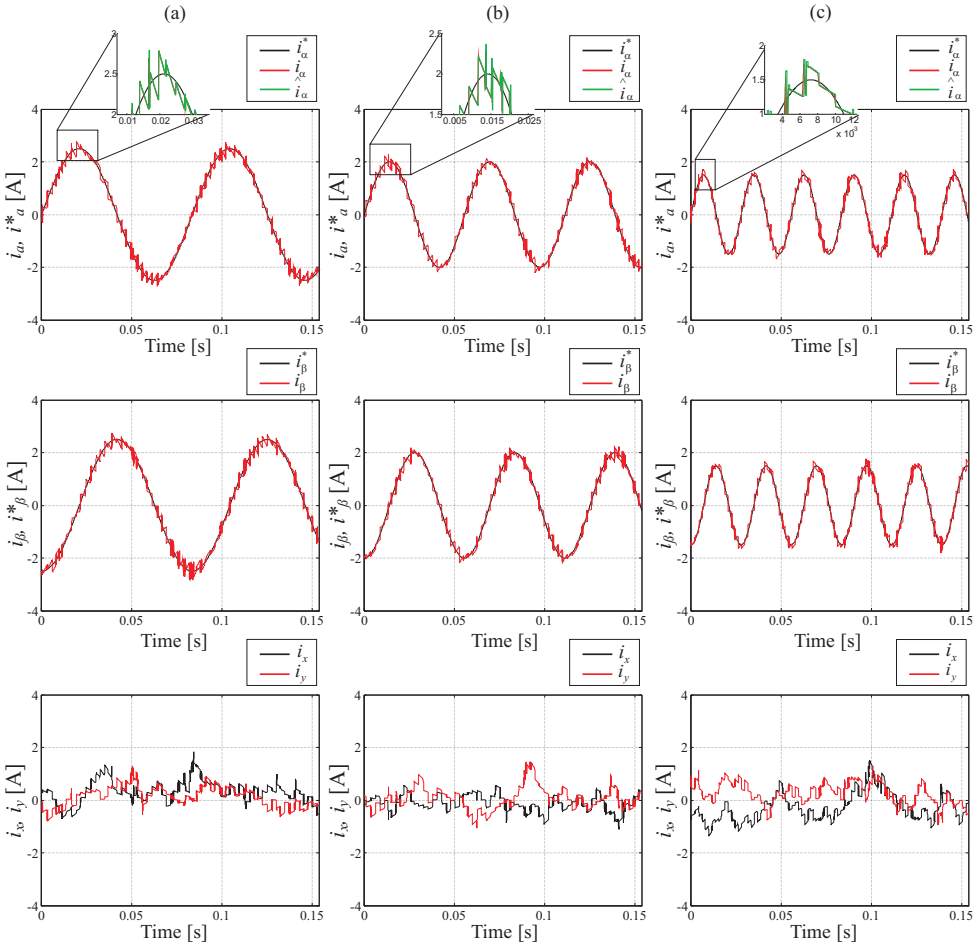

Figure 5. Stator current in $(\alpha - \beta)$ component tracking and $(x - y)$ current components. (a) 2.5 A (peak) current reference at 12 Hz. (b) 2 A current reference at 18 Hz and (c) 1.5 A current reference at 36 Hz

a. The MBPC is a flexible approach that, opposite to PWM based control methods, allows a straightforward generalization to different requirements only changing the cost function

b. The MBPC method is discontinuous technique, so the switching frequency is unknown. This feature reduces the switching losses (compared to continuous techniques) at expense of an increase in the harmonics of the stator current

c. As increases the frequency of the reference currents the switching frequency decreases, consequently there is a degradation in the THD of the stator currents as can be seen in Table 4

4.2. Proposed speed control method

The structure of the proposed speed control for the asymmetrical dual three-phase induction machine based on a KF is shown in Figure 6. The process of calculation of the slip frequency (ω_{sl}) is performed in the same manner as the Indirect Field Orientation methods, from the reference currents in dynamic reference frame (i^*_{ds}, i^*_{qs}) and the electrical parameters of the machine (R_r, L_r) [13, 14]. The inner loop of the current control, based on the MBPC selects control actions solving an optimization problem at each sampling period using a real system model to predict the outputs. As the rotor current can not be measured directly, it should be estimated using a reduced order estimator based on an optimal recursive estimation algorithm from the Equations 21-24.

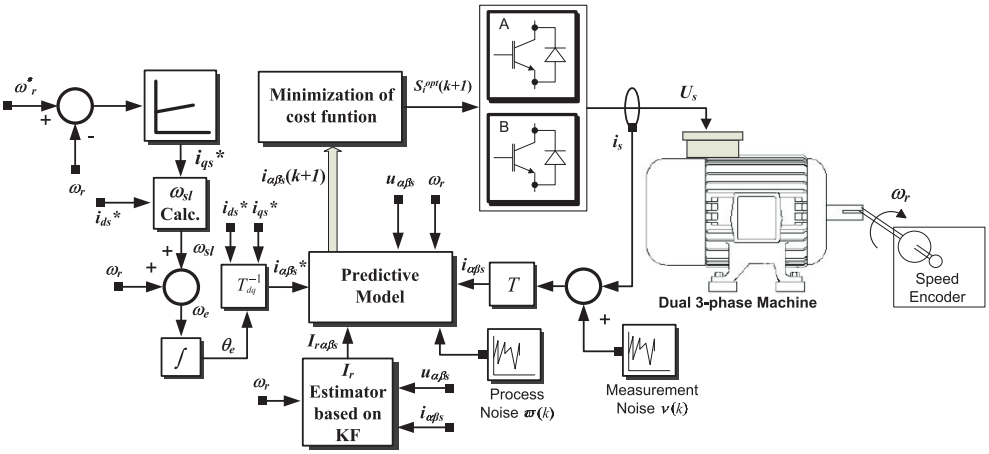

Figure 6. Proposed speed control technique based on KF for the asymmetrical dual three-phase induction machine

Different cost functions (J) can be used, to express different control criteria. The absolute current error, in stationary reference frame $(\alpha - \beta)$ for the next sampling instant is normally used for computational simplicity. In this case, the cost function is defined as Equation 25, where i^*_s is the stator reference current and $i_{\alpha\beta}(k+1|k)$ is the predicted stator current which is computationally obtained using the predictive model. However, other cost functions can be established, including harmonics minimization, switching stress or VSI losses [6]. Proportional integral (PI) controller is used in the speed control loop, based on the indirect vector control schema because of its simplicity. In the indirect vector control scheme, PI speed controller is used to generate the reference current i^*_{ds} in dynamic reference frame. The current reference used by the predictive model is obtained from the calculation of the electric angle used to convert the current reference, originally in dynamic reference frame $(d - q)$, to static reference frame $(\alpha - \beta)$ as shown in Figure 6.

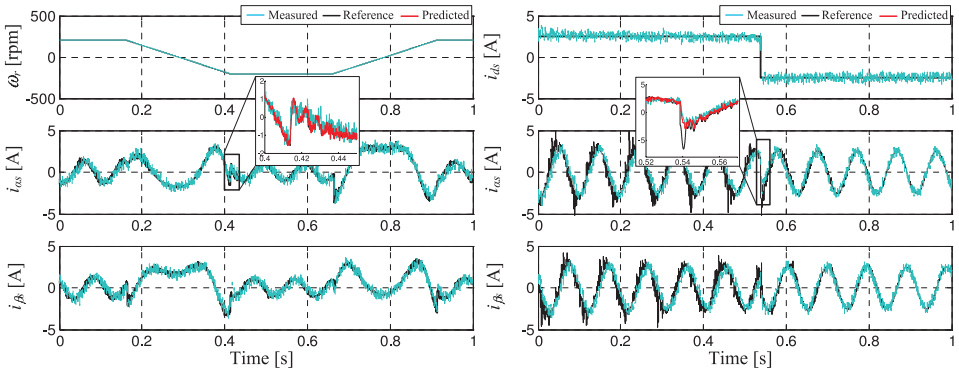

(a) Simulation results for a ±320 rpm step wave speed comand tracking

(b) Simulation results for a ±2.5 A step in the reference current comand tracking

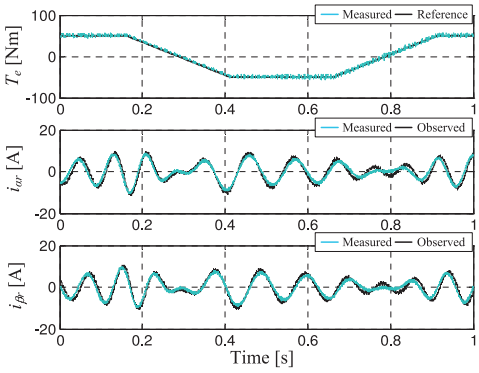

(c) Simulation results for a 50 Nm trapezoidal load

Figure 7. Simulation results for a proposed speed control. The predicted stator current in the α component is shown in the upper side (zoom graphs, red curves)

Figure 7 (a) shows simulation results for a 200 revolutions per minute (rpm) trapezoidal speed reference, if we consider a fixed current reference ($i_{ds}^{*} = 1$ A). The subscripts $(\alpha - \beta)$ represent quantities in the stationary frame reference of the stator currents. The measurement speed is fed back in the closed loop for speed regulation and a PI controller is used in the speed regulation loop as shown in Figure 6. The predicted stator current in the α component is shown in the upper side (zoom graph, red curve). Under these test conditions, the MSE in the speed and current tracking are 0.75 rpm and 0.15 A, respectively. Figure 7 (b) shows the step response for the induction machine to a change of ±2.5 A in the current reference (i_{ds}^{*} see Figure 6), if we consider a fixed speed reference ($\omega_r^{*} = 200$ rpm). In these simulation results, the subscripts $(\alpha - \beta)$ represent the stator current in stationary reference frame. Under these test conditions, the MSE in the stator current tracking are 0.1 A for the reference current (i_{ds}^{*}) and 0.18 A considering stationary reference frame. Finally, Figure 7 (c) shows a trapezoidal load application response, and the rotor current evolution (measured and observed) in stationary reference frame. These simulation results substantiate the expected

performance of the proposed algorithm, based on a Kalman Filter. The estimated rotor current converges to real values for these test conditions as shown in figures, proving that the observer performance is satisfactory.

5. Conclusions

In this chapter a new approach for the speed control of the asymmetrical dual three-phase induction machine has been proposed and evaluated. The speed control scheme uses an inner loop predictive current control based on the model, where the main advantage is the absence of modulation techniques. The MBPC is described using a state-space representation, where the rotor and stator current are the states variables. The proposed algorithm provides an optimal estimation of the rotor current in each sampling time in a recursive manner, even when internal parameters of the drive are not precisely known, and the measurements of the state variables are perturbed by gaussian noise. The theoretical development based on a Kalman Filter has been validated by simulations results. The method has proven to be efficient even when considering that the machine is operating under varying load regimes.

Acknowledgments

The author gratefully the Paraguay Government for the economical support provided by means of a Conacyt Grant (project 10INV01). Also, wishes to express his gratitude to the anonymous reviewers for their helpful comments and suggestions.

Author details

Raúl Igmar Gregor Recalde
Engineering Faculty of the National University of Asunción
Department of Power and Control Systems, Asunción-Paraguay

6. References

[1] Levi, E. (2008). Multiphase electric machines for variable-speed applications. *IEEE Transactions on Industrial Electronics*, Vol. 55, No. 5, (May 2008) page numbers (1893-1909), ISSN 0278-0046

[2] Bucknal R. & Ciaramella, K. (2010). On the Conceptual Design and Performance of a Matrix Converter for Marine Electric Propulsion. *IEEE Transactions on Power Electronics*, Vol. 25, No. 6, (June 2010) page numbers (1497-1508), ISSN 0885-8993

[3] Zhao Y. & Lipo, T. (1995). Space vector PWM control of dual three-phase induction machine using vector space decomposition. *IEEE Transactions on Industry Applications*, Vol. 31, No. 5, (October 1995) page numbers (1100-1109), ISSN 0093-9994

[4] Boglietti, A.; Bojoi, R.; Cavagnino, A.& Tenconi, A. (2008). Efficiency Analysis of PWM Inverter Fed Three-Phase and Dual Three-Phase High Frequency Induction Machines for Low/Medium Power Applications. *IEEE Transactions on Industrial Electronics*, Vol. 55, No. 5, (May 2008) page numbers (2015-2023), ISSN 0278-0046

[5] Arahal, M.; Barrero, F.; Toral, S.; Durán, M.; & Gregor, R. (2008). Multi-phase current control using finite-state model-predictive control. *Control Engineering Practice*, Vol. 17, No. 5, (October 2008) page numbers (579-587), ISSN 0967-0661

[6] Barrero, F.; Arahal, M.; Gregor, R.; Toral, S. & Durán, M. (2009). A proof of concept study of predictive current control for VSI driven asymmetrical dual three-phase AC machines. *IEEE Transactions on Industrial Electronics*, Vol. 56, No. 6, (June 2009) page numbers (1937-1954), ISSN 0278-0046

[7] Barrero, F.; Prieto, J.; Levi, E.; Gregor, R.; Toral, S.; Duran, M. & Jones, M. (2011). An Enhanced Predictive Current Control Method for Asymmetrical Six-phase Motor Drive. *IEEE Transactions on Industrial Electronics*, Vol. 58, No. 8, (Aug. 2011) page numbers (3242-3252), ISSN 0278-0046

[8] Gregor, R.; Barrero, F.; Toral, S.; Duran, M.; Arahal, M.; Prieto, J. & Mora, J. (2010). Predictive-space vector PWM current control method for asymmetrical dual three-phase induction motor drives. *IET Electric Power Applications*, Vol. 4, No. 1, (January 2010) page numbers (26-34), ISSN 1751-8660

[9] Duran, M.; Prieto, J.; Barrero, F. & Toral, S. (2011). Predictive Current Control of Dual Three-Phase Drives Using Restrained Search Techniques. *IEEE Transactions on Industrial Electronics*, Vol. 58, No. 8, (Aug. 2011) page numbers (3253-3263), ISSN 0278-0046

[10] Shi, K.L.; Chan, T.F.; Wong, Y.K. & Ho, S.L. (2002). Speed estimation of an induction motor drive using an optimized extended Kalman filter. *IEEE Transactions on Industrial Electronics*, Vol. 49, No. 1, (Feb. 2002) page numbers (124-133), ISSN 0278-0046

[11] Franklin, G.; Powell, J. & Workman, M. (1998). Optimal Estimation. The Kalman Filter, In: *Digital Control of Dynamic Systems*, Addison - Wesley, (Ed. 3rd), page numbers (389-392), ISBN 978-0-201-82054-6

[12] Vargas, R.; Cortes, P.; Ammann, U.; Rodriguez, J. & Pontt, J. (2007). Predictive Control of a Three-Phase Neutral-Point-Clamped Inverter. *Transactions on Industrial Electronics*, Vol. 54, No. 5,(Oct. 2007), page numbers (2697-2705), ISSN 0278-0046

[13] Ong, C.M. (1997). Indirect Field Orientation Methods, In: *Dynamic Simulation of Electric Machinery Using MatLab/Simulink*, Prentice Hall, page numbers (439-440), ISBN 978-0-137-23785-2

[14] Krause, P.; Wasynczuk, O. & Sudhoff, S. (2002). Indirect Rotor Field-Oriented Control, In: *Analysis of Electric Machinery and Drive Systems*, Wiley-IEEE Press, (Ed. 2nd) page numbers (550-554), ISBN 978-0-471-14326-0